Numerical Analysis of Various Horizontal Axis Wind Turbine Blades and Optimization for Low Wind Velocity

Ali Akbor Topu, Raju Ahammad *

Department of Mechanical Engineering, Khulna University of Engineering & Technology, Khulna-9203, BANGLADESH

ABSTRACT

Among different renewable energy sources, wind energy is a promising source for harvesting energy, but the main obstacle here is that the wind velocity is not high enough everywhere. Small-scale wind turbine blade output is very small as the power output of wind power is proportional to the square of air velocity. Therefore, research is going on to develop new blades efficient enough to produce electricity at low wind velocity by optimizing blade shape. In this study, two airfoil models NACA 63-415 and NACA 63-412 were analyzed numerically using ANSYS Fluent software. Different aerodynamic properties such as static pressure, dynamic pressure, velocity magnitude, and streamlines were observed. At velocity inlet, the upstream velocity of air is 3m/s for Re=200000. The velocity components are calculated for each angle of attack. For velocity inlet boundary condition turbulence intensity is considered 1% and for pressure outlet boundary is 5%. In addition, a turbulence viscosity ratio of 10 is used for better approximation. At different angles of attack [0-18 degree] lift coefficient, drag coefficient, thus, the optimum angle of attack is measured. Blade sections made by the same airfoils are optimized by changing the twist angle. The blade section is twisted from 0 to 16 degrees on a 4 degrees interval. Therefore, the optimum twist angle is calculated 12 degrees where the lift coefficient is maximum compared with the drag coefficient.

Keywords: Wind Turbine, NACA 63-415, NACA 63-412, Turbulence, Optimization

1. Introduction

Human civilization starts flourishing when they learn how to make fire. From the past to the present, energy usage never declined rather than increased exponentially. In the modern era of science and technology, human kind is greatly in need of more power than ever before, and to meet this energy, we are greatly dependent on the use of fossil fuels. Though fossil fuels meet most of our energy demand, they are not abundant enough and contribute to serious environmental issues like global warming. Climate change due to global warming raises serious concerns for the very existence of humankind. Therefore, renewable energy is the best solution to our energy problem [1].

Renewable energy sources like solar, wind, geothermal, and biogas are playing a tremendous role in the mitigation of the energy crisis, especially wind energy is a reliable source for harnessing clean energy. Wind energy is available in every corner of the world and is more economically viable source for power generation. Furthermore, it can be used in remote, isolated places where a central electric grid connection is not available. Therefore, wind energy is a promising source for achieving the sustainable development goal of clean energy for all [2].

Wind turbine blades are the most vital part of the wind energy system, and they are categorized as two types based on their axis of rotation. They are the horizontal axis wind turbine (HAWT) and the vertical axis wind turbine (VAWT). They each have their advantages and disadvantages. HAWT is more advantageous in terms of its power output, efficiency, and reliability than VAWT, which uses the drag force resulting in low efficiency. Furthermore, yaw control allows HAWT to achieve higher efficiency. The large-scale wind turbine can produce electricity from several hundred KW to

10 MW electricity, whereas small-scale concerns within 20 KW electricity production. A large-scale wind turbine is suitable only for coastal and isolated areas [3]. On the contrary, a small-scale wind turbine can be installed anywhere, even on a rooftop. The wind velocity is typically as low as 3 m/s in Bangladesh. Thus, the small-scale wind turbine is suitable for power generation in Bangladesh.

Wind turbine blades comprise different models of airfoils, such as NACA, SG, SERI, etc. The aerodynamic characteristics of these airfoils are the main concern in developing more efficient wind turbines. The performance of an airfoil of HAWT can be improved by increasing the lift to drag co-efficient. Therefore, computational fluid dynamics (CFD) is utilized to analyze the aerodynamic parameters [4].

In the present work, the performance parameters and aerodynamic properties are analyzed and compared with two NACA airfoils using 2D CFD simulations and validated with the experimental data from the literature. Furthermore, blade sections with different twist angles are analyzed by using 3D CFD simulations.

Wind power has a long history in Persia (present-day Iran), dating back to 500–900 AD. A battery charging machine, installed by James Blyth in Scotland in July 1887, was the first electricity-generating wind turbine. After a few months, American inventor Charles F. Brush was able to construct the first automatic wind turbine. Denmark's mechanics developed a 22 kW micro turbine in the early 1990s [5].

In 2010, T. Letcher designed a wind turbine which is an amalgamation of shared vertical axis turbines. Savonious and Darrieus rotors are used. At lower wind speeds, the turbine's total power is increased by the design [6]. In 2011, S.O. Ani reviewed a couple of small-scale wind turbine

---

systems that are commercially available. In a low wind speed climate, the analysis is calculated on the basis of energy output per swept area and cost per generated power [7].

In 2012, H.G. Briggs focused on designing a 1 kW range of wind turbines for small houses or remote institutes. He estimated the overall turbine design and the generator's initial specifications for a household demand [8]. In 2013, P. Pathike developed a turbine model based on blade element momentum theory with an FD 2.7-500 wind turbine for low wind speed operation of 6m/s and efficiency of 27% [9].

In 2015, R.H Barnes analyzed the comparative structure of generic blades from high and low wind speed turbines. He improved the design for low wind blades with more emphasis on stiffness. This results in a lighter and cheaper blade [10]. In 2016, M. Mohammadi proposed a new optimization method for blades where the objective function is maximum output torque, and about 19.5 percent of the torque can be increased [11].

There is research going on low velocity wind turbines nowadays. Here, this paper mainly focuses on the numerical study of the aerodynamic characteristics of NACA63-415 and NACA63-412, which are used to design turbine blades for low-speed wind turbines and optimize the blade section by selecting the best twist angle.

2. Numerical Methodology

2.1 Computational Methodology

Navier-Stokes are the basic governing equation for a viscous fluid. Navier-Stokes equation for incompressible steady flow can be defined as-

X-momentum:

$$u\frac{\partial u}{\partial x} + v\frac{\partial u}{\partial y} = -\frac{\partial p}{\partial x} + \frac{1}{Re}\left[\frac{\partial \tau_{xx}}{\partial x} + \frac{\partial \tau_{xy}}{\partial y}\right] \quad (1)$$

Y-momentum:

$$u\frac{\partial v}{\partial x} + v\frac{\partial v}{\partial y} = -\frac{\partial p}{\partial u} + \frac{1}{Re}\left[\frac{\partial \tau_{xy}}{\partial x} + \frac{\partial \tau_{yy}}{\partial y}\right] \quad (2)$$

For the two-dimensional steady flow, continuity equation is,

$$\frac{\partial u}{\partial x} + \frac{\partial v}{\partial y} = 0 \quad (3)$$

Numerical simulation was done using four different turbulence models namely Spalart-Allmaras, K-epsilon, K-omega, and Transitional SST with fixed Reynolds number, and compared with experimental data which is taken from a scientific paper as described in section 2.9.

2.2 Geometry

In order to precisely plot the profile of NACA 63-415 and NACA 63-412, co-ordinates are collected from online profile generator for NACA 6-digit airfoil series [12]. The blade section was drawn in Solidworks software. The blade section span length is 5.08 cm and the chord length is 2.54 cm as shown in Fig. 1. The angle between the left and the right plane is twist angle. Here, 5 blades are used consisting of 0°, 4°, 8°, 12°, 16° twist angles respectively.
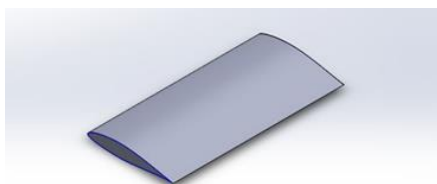

Fig. 1 3D view of blade section

2.3 Computational domain

The geometry utilized in the simulation is created by importing NACA63-415 coordinates as points. A curve is formed from the points. With a 1 m chord length, a surface that resembles NACA 63-415's cross section is generated. Then, in the same plane as the airfoil, a C mesh domain is formed by drawing the C mesh. Then the C mesh is split into four quadrants to help control the mesh size at the surface. The airfoil is subtracted from the main semi-circular portion. The computational domain comprised 12.5C above the pressure surface, 12.5C upstream of the leading edge, and 12.5C downstream of the trailing edge of the airfoil.

2.4 Grid generation and wall treatment

In this work, flow domains are separated into smaller subdomains in order to investigate fluid flow. Within each of these subdomains, the governing equations are discretized and solved. The meshing precision increases as we go closer to the airfoil, as seen in Fig. 2.
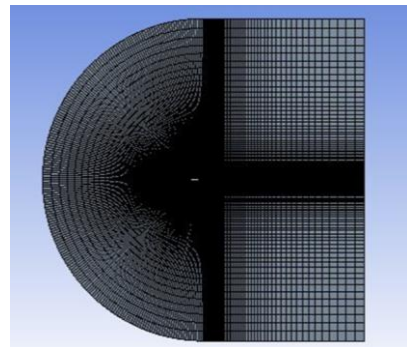

Fig. 2 Close view of the mesh around NACA 63-415 airfoil

The flow field of the airfoil is discretized using a C-type mesh constructed using the quadrilateral approach. There are 40,000 elements in the C-type grid. The biasing approach is used to obtain accuracy in the near wall or airfoil area. In addition, wall treatment is carried out. NACA 63-412 follows the same procedures. y+ values are ensured to less than one in the whole domain.

A rectangular domain is selected for analyzing the blade section. The enclosure command is used for this. The dimension of every arm of the rectangle is 20 cm. The meshing precision increases as moving closer to the blade, as illustrated in Fig. 3. Face sizing, inflation and sphere of influence are used to generate fine mesh around the blade.
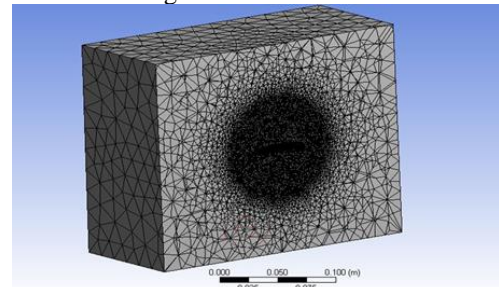

Fig. 3 Mesh around Blade

2.5 Boundary Conditions

The circular arc section is defined as a velocity inlet, the two outer horizontal lines are defined as pressure far field and the last two vertical lines are defined as pressure outlet

which is shown in Fig. 2. At velocity inlet, the upstream velocity of air is 3m/s for Re = 200000. Turbulence intensity is assumed to be 1% for the velocity inlet boundary and 5% for the pressure outlet boundary. In addition, for better approximation, a turbulence viscosity ratio of 10 is applied.

For the blade section, the left wall is treated as a velocity inlet and the right wall is treated as a pressure outlet. All the other walls are treated as pressure far field. At velocity inlet, the upstream velocity of air is 3m/s and the angle of attack is zero degree.

2.6 Solver setting

Pressure based couple solver was used by SIMPLE method. All of the equations (pressure, momentum, and turbulence) were solved using a second-order upwind spatial discretization approach, while gradients were solved using a least squares cell-based technique. Whenever the residuals drop below a threshold of 10^{-06}, the simulation process is said to be converged. Air is selected as the fluid material and the operating pressure to the ambient value of 101325 Pa.

2.7 Mesh dependency test

For five different mesh settings, the simulation was run to test the independency of the selected domain. The result was found as follows in Table 1.

Table 1 Data for mesh dependency test

Mesh Element	Max Static Pressure, (pa)	Max Velocity Magnitude, (m/s)
10000	4.9824	3.8224
22500	5.0412	3.8358
28900	5.3539	3.8380
40000	5.4366	3.8416
52900	5.4369	3.8417

It is seen that number for elements number 40000 and 52900 the maximum velocity magnitude on the flow field shows a similar magnitude. Thus, for the further simulation process, the domain that contains 40000 elements had been chosen as a standard domain.

2.8 Result Validation

As seen in Fig. 4, the dimensionless lift coefficient increased linearly with the angle of attack for low angles of attack. The flow on the upper surface of the airfoil started to separate at about 15 to 16 degrees angle of attack, and a stall developed. The lift coefficient is reduced as a result of the strong flow separation at the stall angle of attack. Similarly, Fig. 5, Fig. 6 and Fig. 7 show the validation for the simulation.
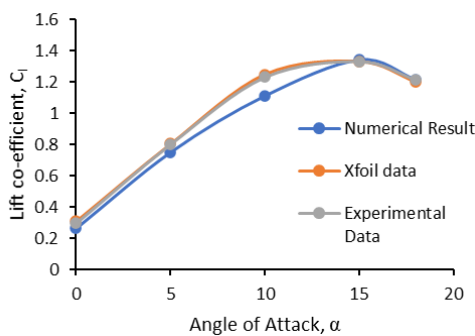

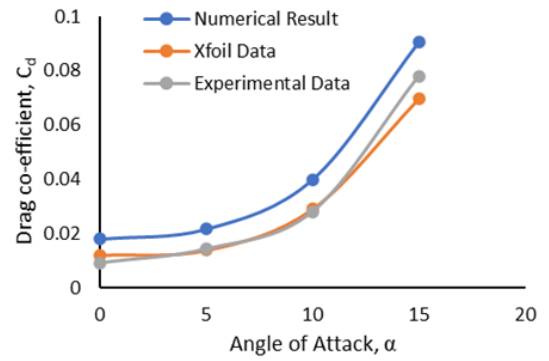**Fig. 4** Lift co-efficient vs AOA for experimental data [13], Xfoil data [12] and numerical result for NACA 63-415

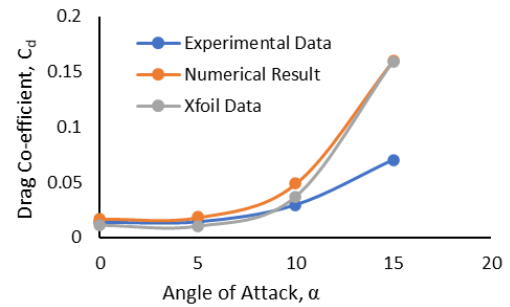**Fig. 5** Drag co-efficient vs AOA for experimental data [13], numerical result and Xfoil data [12] for NACA 63-415

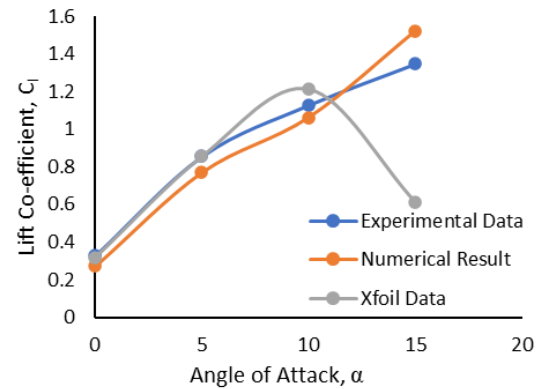**Fig. 6** Drag co-efficient vs AOA for experimental data [13], numerical result and Xfoil data [14] for NACA 63-412

Fig. 7 Lift co-efficient vs AOA for experimental data [13], numerical data, and Xfoil data [14] for NACA 63-412

2.9 Selection of turbulence model

To analyze the flow over NACA 63-415 airfoil, SA, K-Epsilon RNG Enhanced wall, SST K-Omega, Transitional SST turbulence models are used.
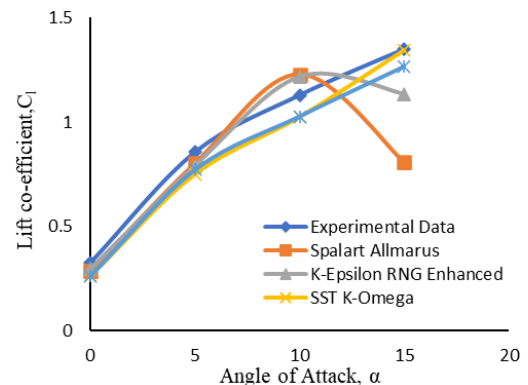

Fig. 8 Comparison of lift coefficient among turbulence models with experimental data [13].
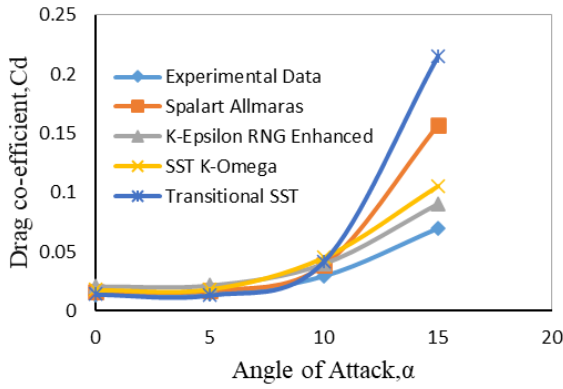
Fig. 9 Comparison of lift coefficient among turbulence models with experimental data [13].

Fig. 8 and Fig. 9 show the SST k-omega model gives correct results than the other turbulence model. So, further results are taken using this turbulence model. Although the k-epsilon method gives a more accurate drag coefficient but not for the lift co-efficient.

3. Result and Discussion

3.1 Static Pressure

Fig. 10 shows there is a region of low pressure on the upper surface and a region of high pressure at the leading edge on the airfoil. For the 0° angle of attack from Fig. 10, it is attained that the contours of static pressure over an airfoil are not symmetrical for both upper and lower surfaces and as a result, there is a certain amount of lift at 0° angles of attack. For the 5° angle of attack, it can be observed that the flow has a stagnation point right under the leading edge, resulting in lift due to a low-pressure zone on the airfoil's upper surface. The high-pressure zone travels towards the bottom surface of the airfoil as the angle of attack increases, while the low-pressure region moves forward. As a result, it is seen that Bernoulli's principle stands true: the velocity is high (as indicated by the red outlines) in the low-pressure zone and vice versa in the high-pressure region.
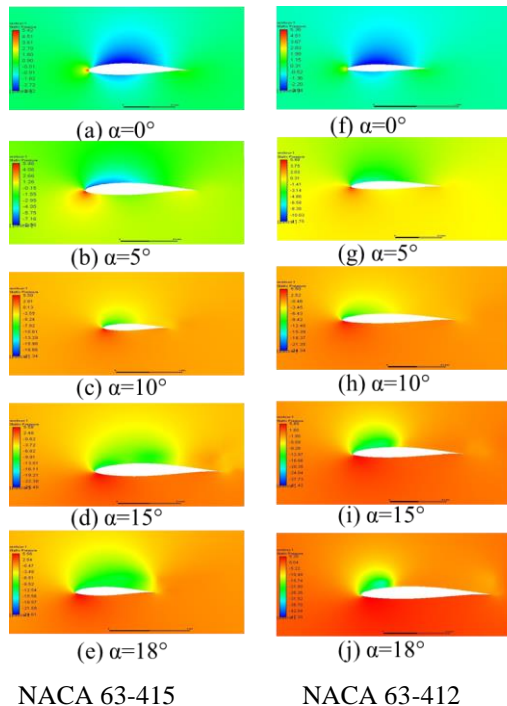

Fig. 10 Static pressure contour at different AOA for NACA 63-415 and NACA 63-412

3.2 Dynamic pressure and velocity magnitude

In Fig. 11 and Fig. 12, contours of dynamic pressure and velocity magnitude are shown for different angles of attack at 3 m/s velocity. As dynamic pressure is a function of velocity, the characteristics are quite similar for both dynamic pressure and velocity magnitude. From 5 degrees angle of attack, the stagnation-point shifts slightly towards the trailing edge via the bottom surface, resulting in a low-velocity region at the lower side of the airfoil and a higher velocity acceleration region at the upper side of the airfoil, and according to Bernoulli's principle, the upper surface will gain low pressure and the lower surface will gain higher pressure. As a result, the value of the coefficient of lift will increase, as will the coefficient of drag, but the increase in drag will be less than the increase in lift. The distribution of velocity, and consequently, the pressures along both surfaces would have been precisely the same in a symmetrical airfoil at no incidence, canceling each other out and resulting in a total lift force of zero. However, because the NACA 63-415 is a non-symmetrical airfoil, the pressure and velocity distribution along both surfaces is not the same. As a result, even if there is no occurrence, a certain amount of lift is created.
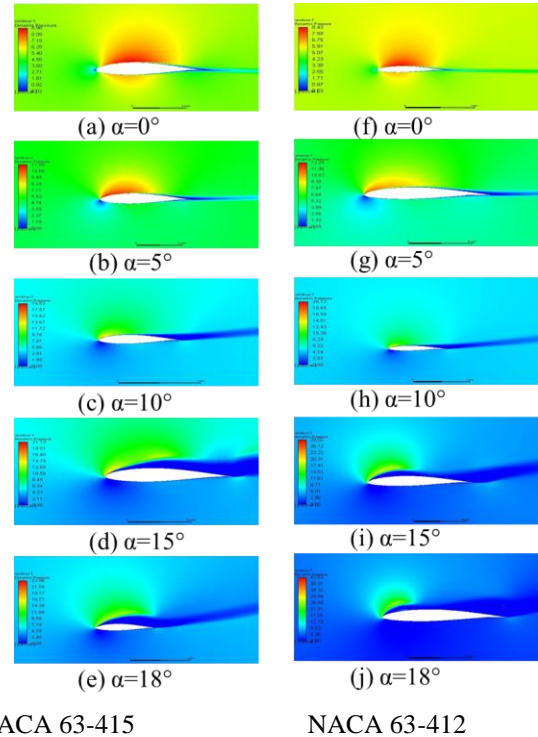

Fig. 11 Dynamic pressure contour at different AOA for NACA 63-415 and NACA 63-412

3.3 Velocity streamline

Fig. 13 depict the flow field over NACA 63-415 and NACA 63-412 airfoils at various angles of attack. The streamlines for various angles of attack are depicted here. The streamlines remain generally undisturbed from their free stream forms at low angles of attack, and C_l is low. Due to the creation of vorticity, the streamlines display a considerable upward deflection in the region of the leading edge and a subsequent downward deflection in the region of the following edge as the angle climbs to 10° and then 15°. As α is increased, the stagnation-point shifts downstream of the leading edge over the bottom surface of the airfoil. C_l rises in sync with α, and the rate of growth is linear. However,
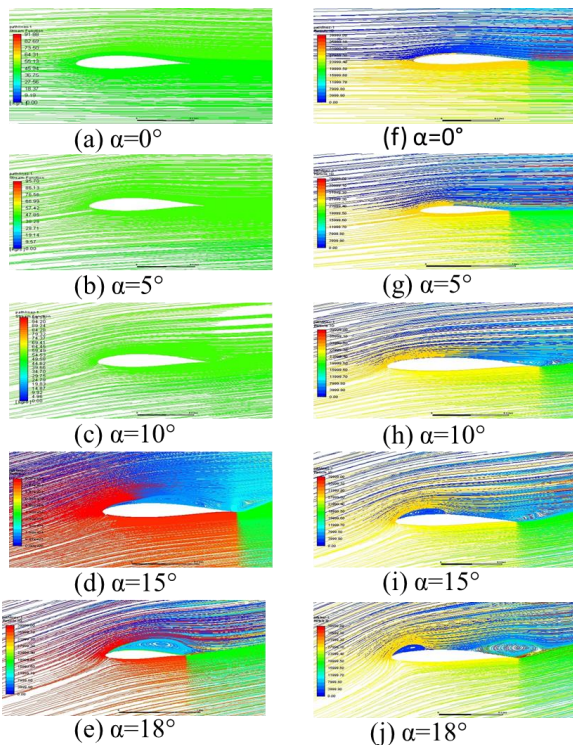
as the angle of attack is raised above 15°, flow separation on the trailing edge of the airfoil becomes slow and progressive. The separation bubble grows larger as a result of the rise in α, as illustrated in Fig. 13.
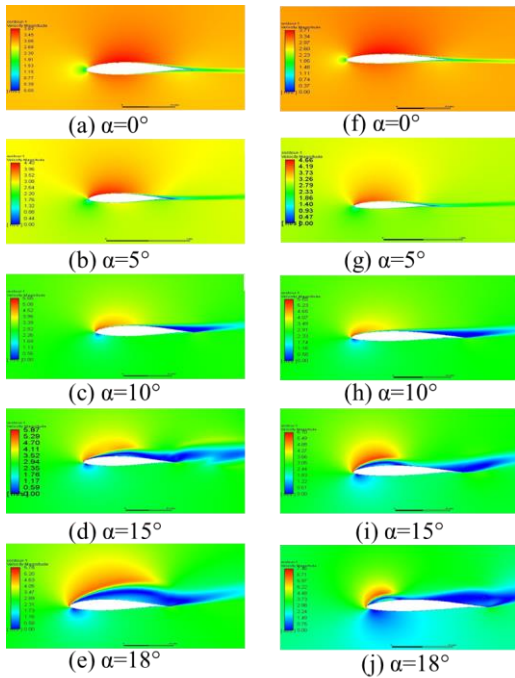
Fig. 12 Velocity magnitude contour at different AOA for NACA 63-415 and NACA 63-412

Fig. 13 Velocity streamline at different AOA for NACA 63-415 and NACA 63-412

3.4 Blade Optimization

The blade of a wind turbine consists of different airfoils. Here in this paper, the blade shape is optimized by selecting the best twist angle at which the lift coefficient is higher. Fig. 14 shows the relation between the lift coefficient and twist angle. The lift coefficient increases with the twist angle and the highest value is got at a 12° twist angle. After that lift co-efficient is started to decrease due to the flow separation.
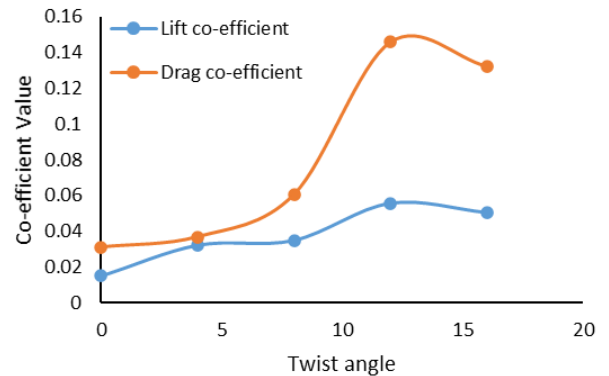

Fig. 14 Relation between lift and drag co-efficient with twist angle

4. Conclusion

The main goal of this paper was to investigate the influence of aerodynamic features of NACA 63-415 and NACA 63-412 airfoils at different angles of attack and at the same Reynolds number and wind velocity using Ansys Fluent CFD software. An investigation of the influence of the angle of attack on the aerodynamic performance of a small-scale wind turbine airfoil was carried out by CFD with four turbulence models. Airfoil NACA 63-415 was simulated and results were compared with verified data. In this paper, a small-scale wind turbine blade section was modified by changing the twist angle. And the optimum twist angle is selected. So, the outcomes of this paper are discussed below-

1. Lift coefficients were calculated for different angles of attack. The optimum lift co-efficient for NACA 63-415 is 1.2142 at 15° angle of attack.
2. The coefficients of drag (C_d) and lift (C_l) were computed and compared to the experimental data, which revealed a similar likeness, indicating that the research was legitimate.
3. Optimum twist angle is 12° for a 5cm small-scale wind turbine blade section.

References

[1]. Tong, W., *Wind power generation and wind turbine design*. 2010: WIT press.
[2]. Cassola, F. and M. Burlando, *Wind speed and wind energy forecast through Kalman filtering of Numerical Weather Prediction model output*. Applied energy, 2012. 99: p. 154-166.
[3]. Sagol, E., M. Reggio, and A. Ilinca, *Assessment of two-equation turbulence models and validation of the performance characteristics of an experimental wind turbine by CFD*. International Scholarly Research Notices, 2012. 2012.
[4]. Patel, M.B. and D. Patel, *A Review on Aerodynamic Analysis of Wind Turbine Blade Using CFD Technique*. International Journal of Engineering Research & Technology (IJERT), 2012. 1(10): p. 2278-0181.

[5]. Wikipedia. *Wind turbine*. 2022 [cited 2022 14-10-2022]; Available from: https://en.wikipedia.org/wiki/Wind_turbine.

[6]. Letcher, T., *Small scale wind turbines optimized for Low Wind Speeds*. 2010.

[7]. Ani, S., H. Polinder, and J. Ferreira. *Energy yield of small wind turbines in low wind speed areas*. in *3rd IEEE International Conference on Adaptive Science and Technology (ICAST 2011)*. 2011. IEEE.

[8]. Gitano-Briggs, H., *Low speed wind turbine design*. Advances in Wind Power, 2012.

[9]. Pathike, P., et al., *Small horizontal-axis wind turbine blade for low wind speed operation.* Journal of Applied Science and Engineering, 2013. 16(4): p. 345-351.

[10]. Barnes, R., E. Morozov, and K. Shankar, *Improved methodology for design of low wind speed specific wind turbine blades.* composite structures, 2015. 119: p. 677-684.

[11]. Mohammadi, M., et al., *Optimization of small-scale wind turbine blades for low-speed conditions.* Journal of Clean Energy Technologies, 2016. 4(2): p. 140-143.

[12]. Tools, A. 2020 14-10-2022]; Available from: http://airfoiltools.com/airfoil/details?airfoil=n63415-il#polars.

[13]. Bak, C., et al., *Wind tunnel tests of the NACA 63-415 and a modified NACA 63-415 airfoil.* 2000.

[14]. *Airfoil Tools*. 2022 [cited 2022 14-10-2022]; Available from: http://airfoiltools.com/airfoil/details?airfoil=n63412-il#polars.

NOMENCLATURE

C_d : coefficient of drag

C_l : coefficient of lift

α : angle of attack, ° (Degree)